Antiferromagnetic defect structure in LaNiO$_{3-\delta}$ single crystals

Bi-Xia Wang,[1] S. Rosenkranz,[1] X. Rui,[2] Junjie Zhang,[1,3] F. Ye,[4] H. Zheng,[1] R. F. Klie,[2] J. F. Mitchell,[1,*] and D. Phelan[1,†]

[1]*Materials Science Division, Argonne National Laboratory, Argonne, Illinois 60439, USA*
[2]*Department of Physics, University of Illinois at Chicago, Chicago, Illinois 60607-7061, USA*
[3]*Materials Science and Technology Division, Oak Ridge National Laboratory, Oak Ridge, Tennessee 38731, USA*
[4]*Neutron Scattering Division, Oak Ridge National Laboratory, Oak Ridge, Tennessee 37831, USA*

The origins of the metal-insulator and magnetic transitions exhibited by perovskite rare-earth nickelates, RNiO$_3$ (where R is a rare-earth element), remain open issues, with charge disproportionation, magnetic interactions, and lattice response across multiple length scales being among the many possible origins. Recently, growth of single crystals of LaNiO$_3$, which is the only member of these compounds that remains metallic in its ground state, has been reported, opening a new chapter in the investigation of the perovskite nickelates. Here, using a combination of magnetometry, heat capacity, and neutron scattering on as-grown and purposely reduced LaNiO$_{3-\delta}$ crystals, we show that both antiferromagnetic and ferromagnetic phases with a Néel temperature of ∼152 K and a Curie temperature of ∼225 K can be induced by reduction of the oxygen content. Transmission electron microscopy shows that these phases are characterized by ordered oxygen vacancy defect structures that exist as dilute secondary phases in as-grown crystals despite growth in partial oxygen pressures up to at least 130 bar. The demonstration of antiferromagnetism resulting from oxygen vacancy ordered structures implies that stoichiometry must be explicitly considered when interpreting the bulk properties of LaNiO$_{3-\delta}$ single crystals; accordingly, the implications of our results for putative oxygen-stoichiometric LaNiO$_3$ are discussed.

I. INTRODUCTION

Rare-earth perovskite nickelates (RNiO$_3$ where R is a rare-earth element) represent an important series that continues to challenge our understanding of how magnetic order and electrical transport behave in transition-metal oxides and how they relate to the complex correlations of charges, spins, the lattice, and orbitals. Notably, aside from LaNiO$_3$, all compounds in the series undergo metal-insulator transitions (MIT) and possess insulating, antiferromagnetic (AFM) ground states [1]. These transitions have been shown to correlate with the e_g bandwidth, which is modulated by the R^{3+} ionic radii via Ni-O-Ni bond angles [2]. A structural phase transition ($Pnma$ to $P2_1/n$) occurs simultaneously with the MIT for R ≠ La [3], and this MIT has been discussed in terms of charge disproportionation, Jahn-Teller distortions, charge transfer, covalency, and ligand holes [4–19]. In particular, one interpretation of the MIT is that it arises due to the disproportionation of charge on nickel sites, such that charge order occurs, which breaks the $Pnma$ symmetry in the low-temperature, insulating phase [3,4,8]. Recently, an alternative scenario, which is commonly referred to as bond disproportionation, has received significant attention [11–14]. In this mechanism, ligand holes play an important role such that the transfer of charge between oxygen anions and nickel cations leads to the disproportionation and concomitant inequivalent magnetic moments on charge sublattices [11]. Bond disproportionation has been used to interpret recent

x-ray absorption and resonant inelastic x-ray scattering spectroscopies [14] and has been favored in recent double-cluster calculations [11]. Nevertheless, the mechanism of the MIT continues to be a focus of both experimental and theoretical work in nickelates.

For small bandwidth nickelates (R^{3+} radius <Nd^{3+}), the MIT occurs at a higher temperature than the AFM transition [1], demonstrating that charge and spin are the primary and secondary order parameters, respectively. However, the simultaneous occurrence of AFM and MIT for R = Nd/Pr, opens the question as to whether there is a crossover in the primary and secondary order parameters upon increasing bandwidth [10,20,21]. In this context, it is interesting to consider LaNiO$_3$, which has a behavior that has long been understood to deviate from the remainder of the series. In particular, LaNiO$_3$ has been described as Pauli paramagnetic [22], metallic [22–24], and rhombohedral [24,25] spanning from low (∼4 K) to at least room temperature. Neither MIT [22–24] nor long-range structural phase transitions [25] have been reported, and powder neutron diffraction measurements have to date revealed no evidence of antiferromagnetic ordering [25]. Yet, clearly, this compound lies extremely close to magnetic and structural transitions, and recently experimental and theoretical considerations have cast doubt upon whether the simple picture of a rhombohedral, paramagnetic metallic ground state is appropriate. For example, two recent reports of pair density function analysis of neutron diffraction data [18,19] favor a monoclinic description of the local environment in LaNiO$_3$ to at least 200 K. This would imply charge disproportionation akin to the long-range charge ordered structure that occurs for all other RNiO$_3$ [8,26,27] at least on local length scales.

First-principles calculations indicate that rhombohedral and orthorhombic structures lie very close in energy—indeed, so close that fluctuations between these structures may occur [17]. Breathing modes and antiferromagnetic ordering were both found to be energetically favorable (breathing modes significantly more so) [17].

Whereas the bulk of all previous work has been performed on polycrystalline materials, advances in high-pressure floating-zone growth have recently led to two reports of single crystal growth of $LaNiO_{3-\delta}$, but differing interpretations have led to uncertainty regarding its intrinsic behavior. Zhang *et al.* reported single crystals possessing rhombohedral symmetry, metallic behavior, and no obvious magnetic ordering based on both magnetic susceptibility and heat capacity, although a broad maximum in the susceptibility was observed at ~200 K [28]. On the other hand, Guo *et al.* have reported metallic, rhombohedral single crystals with anomalies in both the heat capacity and magnetic susceptibility occurring at $T_N \sim 157$ K [6]. Consistent with these results, they reported the appearance of magnetic Bragg reflections via single-crystal neutron diffraction below T_N. If Guo *et al.*'s results are borne out, they would lead to a radical and different interpretation of the physics of $LaNiO_3$, which would revise not only our understanding of bulk $LaNiO_3$, but also of thin films [29–32] and heterostructures [33,34].

$LaNiO_3$ may be proximal to an intrinsic quantum critical point [17], so it is especially important to recognize that stoichiometry and defects can also lead to dramatic modifications of the physical properties [35]. Indeed, although single crystals provide meaningful direction-dependent information that cannot be obtained from polycrystalline specimens and are favored for electrical transport studies, the control of stoichiometry and in some cases defects and impurities can, in fact, present a more significant challenge in large oxide crystals than in bulk polycrystalline materials. Both ferromagnetic and AFM oxygen-deficient phases have previously been reported in polycrystalline lanthanum nickelates [35,36] with T_N close to that reported for the $LaNiO_3$ single crystals by Guo *et al* [6]. This led us to explore the effects of oxygen defects in $LaNiO_{3-\delta}$ single crystals. Here, using a combination of magnetometry, heat capacity, and neutron scattering, we report stabilization of not only an AFM minority phase, $LaNiO_{2.5}$, with $T_N \sim 152$ K, but also a ferromagnetic phase, $LaNiO_{2.75}$ with $T_C \sim 225$ K, both of which we have intentionally induced in $LaNiO_{3-\delta}$ via systematic reduction of the oxygen content. The ordering of oxygen vacancies in these minority phases is further demonstrated by transmission electron microscopy (TEM) measurements.

II. EXPERIMENTAL DETAILS

Single crystals of $LaNiO_{3-\delta}$ were grown using a high-pO_2 floating zone furnace (HKZ-1; SciDre GmbH) under 40 bar and 130 bar pO_2 as described in Ref. [28]. As reported previously [28], the oxygen content of a specimen taken from the $LaNiO_{3-\delta}$ single crystals grown under 40 bar pO_2 was determined to be 2.985(3), i.e., $\delta \approx 0.015(3)$ vacancies/formula unit using thermogravimetric analysis (TGA) measurements. We have obtained similar values [$\delta \approx 0.020(2)$] from a TGA study for a specimen taken from a growth under 130 bar pO_2. Thus,

all of our as-grown crystals possess a finite, but small quantity of oxygen deficiency prior to any of our measurements, despite high oxygen pressure growth. Specimens for structural and bulk properties characterization were prepared by extracting from boules of as-grown single crystals. Specifically, for heat capacity and magnetization measurements, a 22.2 mg specimen was extracted from the crystal boule grown under 40 bar pO_2, and neutron scattering was carried out on samples (~1 g) from single crystals grown under both 40 bar and 130 bar pO_2. Heat capacity measurements were performed in a Quantum Design physical property measurement system (PPMS) in the temperature range of 130–190 K. Apiezon-N vacuum grease was employed to fix the crystal to the sapphire sample platform, and addenda measurements were subtracted. Magnetic susceptibility measurements were performed in a Quantum Design magnetic property measurement system (MPMS-3). Field-cooled and zero-field cooled temperature-dependent susceptibility data were collected under an external field of $\mu_0 H = 5.0$ T. Neutron diffraction experiments were performed on CORELLI [37,38], a time-of-flight diffractometer at the spallation neutron source (SNS) located at Oak Ridge National Laboratory (ORNL) that employs a pseudowhite neutron beam and uses cross-correlation to extract the elastic signal. Because of the twinning of the crystals, we employ a pseudocubic notation when indexing peaks with the aristotype perovskite cell that contains one formula unit ($a \sim 3.9$ Å). By design, CORELLI provides an extremely broad wave-vector coverage with a large signal to noise ratio. To further enhance the visibility of weak peaks, data measured in different octants of reciprocal space were symmetrized using Laue class *mmm*. The scattering from both the 40 bar and 130 bar crystals was dominated by a single, large, twinned crystal in each case, and some impurity peaks, three to four orders of magnitude weaker than the dominant crystal's Bragg peaks, were observed. These weak impurity peaks could be easily discriminated from peaks that are intrinsic to the $LaNiO_{3-\delta}$ crystal by whether or not they are commensurate with the dominant structure.

Magnetometry, heat capacity, and neutron scattering experiments were performed on as-grown and oxygen reduced single crystals in order to directly explore the effects of intentionally induced oxygen deficiency. *Crucial to the design of the experiment, the exact same specimens were measured before and after reduction.* Reduction was conducted on a TGA balance (Mettler-Toledo model DSC 1) in a 4% H_2/N_2 gas mixture. The sample was annealed at temperature intervals of 25 °C from 250 °C up to 400 °C, holding for 24 hours at each temperature. The total weight loss (~88 μg) of the 22.2-mg crystal (grown under pO_2 40 bar), which was used for both the magnetometry and heat capacity measurements, provides an estimate of the average stoichiometry of $LaNiO_{2.924(3)}$ post-reduction, assuming a starting stoichiometry of $\delta = 0.015(3)$ [28]. The weight loss (~4.4 mg) of the ~1.14 g crystal grown under 130 bar used for the neutron scattering measurements gives an average stoichiometry of $LaNiO_{2.921(2)}$ post-reduction, assuming a starting stoichiometry of $\delta = 0.020(2)$. We emphasize that these stoichiometry values represent an average from a single region of the grown boules and that a nonuniform oxygen content variation is likely given the floating zone growth. Furthermore, as we discuss below, the reduction of the single crystal almost certainly leads to an inhomogeneous, core-shell

type of structure with the shell likely having significantly more oxygen vacancies than the core.

TEM, including high-resolution phase contrast imaging, electron diffraction and scanning transmission electron microscopy (STEM) imaging was performed on another as-grown single crystal ($pO_2 = 40$ bar). Selected area electron diffraction pattern (SAED) and phase-contrast TEM imaging was used to analyze the direction and periodicity of putative oxygen vacancy ordering, while STEM images were used to directly visualize the oxygen vacancy ordering in LaNiO$_{3-\delta}$ at the atomic scale. The SAED and TEM images were acquired using a JEOL JEM3010 operated at 300 keV. Low-angle annular dark-field (LAADF) and annular bright-field (ABF) images were acquired using a probe aberration-corrected JEOL JEM-ARM 200CF equipped with cold field emission gun. The convergence semiangle for STEM images was 13.4 mrad, and the collection semiangles for LAADF and ABF detectors were set at range of 40–160 and 11–25 mrad, respectively. The LaNiO$_{3-\delta}$ TEM samples were prepared by crushing single crystal LaNiO$_{3-\delta}$ using mortar and pestle following by an ultrasonic treatment in isopropanol and drop-casting on a holey carbon TEM grid. To avoid beam induced artifacts, the samples were not exposed to any Ar$^+$ beam thinning.

III. RESULTS AND DISCUSSION

We begin by considering the nature of the oxygen vacancies present in our as-grown sample that had been prepared under 40 bar pO_2, whose characterization via TGA on a specimen removed from a growth under the same pressure yielded $\delta \sim 0.015(3)$, though we generally expect that there exist variations between specimens due to oxygen inhomogeneities present during floating zone growth. TEM imaging and electron diffraction (Fig. 1) reveal oxygen vacancy ordering in a small concentration of regions. Figure 1(a) shows a low magnification image of a LaNiO$_{3-\delta}$ particle, which contains areas of LaNiO$_3$ for which no oxygen vacancy ordering is detected as well as oxygen vacancy ordered LaNiO$_{3-\delta}$. Figure 1(b) shows an electron diffraction pattern from the region of LaNiO$_3$ for which no vacancy ordering was detected in the (0, 1, 1) orientation. As expected for a crystal in the rhombohedral space group $R\bar{3}c$, the only reflections that are observed that break cubic symmetry occur at the R points of the cubic Brillouin zone ($^1/_2$$^1/_2$$^1/_2$). We note that in principle not all R points are systematically allowed for $R\bar{3}c$, but the presence of multiple scattering (i.e., Renninger effects) in diffraction experiments is well known to cause violations of the systematic absences, and we consider that to be likely here based on our experience with single-crystal diffraction on other rhombohedral perovskites. Figure 1(c) shows an electron diffraction pattern for oxygen vacancy ordered regions LaNiO$_{3-\delta}$, where superlattice reflections are visible at X points (e.g., ($^1/_2$, 0, 0)), M points (e.g., (0, $-^1/_2$, $^1/_2$)), ($^1/_2$, $-^1/_4$, $^1/_4$), and ($^1/_2$, $-^3/_4$, $^3/_4$). The ($^1/_2$, $-^1/_4$, $^1/_4$), ($^1/_2$, $-^3/_4$, $^3/_4$), and (0, $-^1/_2$, $^1/_2$) superlattice reflections have been previously reported for LaNiO$_{2.75}$ by Gonzalez-Calbet *et al.* [39]. Atomic-resolution STEM imaging [Fig. 1(d)] shows an area of oxygen vacancy ordering in LaNiO$_{2.75}$ as well as an area where no oxygen vacancy ordering was detected.

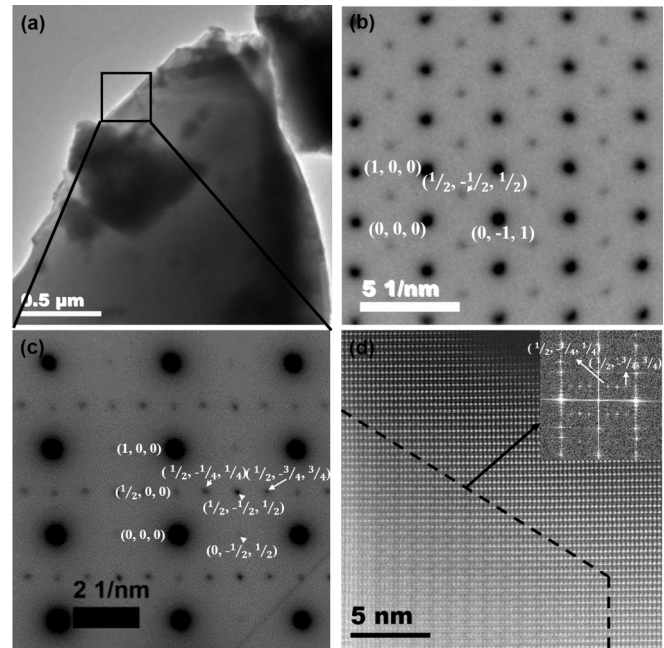FIG. 1. (a) Low-magnification TEM image of an as-grown LaNiO$_{3-\delta}$ sample ($\delta \sim 0.015$). (b) SAED pattern of LaNiO$_3$ for which no oxygen vacancy ordering was detected from the area shown in (a). (c) SAED pattern in the pseudocubic (0,1,1) orientation from different region shown in (a). Superlattice reflections corresponding to the oxygen vacancy ordering are indexed. (d) Atomic-resolution STEM-LAADF image of LaNiO$_{3-\delta}$ showing a domain of oxygen vacancy ordered LaNiO$_{2.75}$ and one where no vacancy ordering could be detected. The fast Fourier transform of the oxygen vacancy ordered domain is shown as an insert. All measurements were performed at room temperature.

It is interesting to note here that we also found areas (see Fig. 1(a) in the Supplemental Material (SM) [40]) where the oxygen vacancies appear to order along the (0, −1, 1) direction, which has been previously reported for LaNiO$_{2.5}$ [35,41–45]. The electron diffraction pattern from this area is shown in Fig. 1(b) of the SM [40] while the corresponding atomic-resolution STEM image is shown in Fig. 1(c) of the SM [40]. In this ABF image, the La, Ni, and O atomic columns are clearly visible, and it can be seen that the oxygen atomic columns show a periodic displacement in every second unit cell along the (0, −1, 1) direction. The vacancy ordering proposed for LaNiO$_{2.5}$ [35,43,45] is shown in Fig. 2 of the SM [40], though we note that consensus is lacking in the literature regarding the proper space group [35,39,41,44,46]. The corresponding SAED pattern shows superlattice reflections at X and M points in agreement with the vacancy-ordered structural motif.

Our TEM analysis shows that two oxygen deficiency structures, LaNiO$_{2.75}$ and LaNiO$_{2.5}$, were present in the as-grown ($pO_2 = 40$ bar) LaNiO$_{3-\delta}$ sample and that the distribution of ordered oxygen vacancies forms small regions of these defect phases. We emphasize here that the electron diffraction pattern for the region identified as LaNiO$_{2.75}$ shows additional superlattice spots at X points [see Fig. 1(c)]. These reflections were not reported by Gonzalez-Calbet *et al.* [39], but they match with the superlattice spots for LaNiO$_{2.5}$. Diffraction patterns from a different region of the same sample are shown
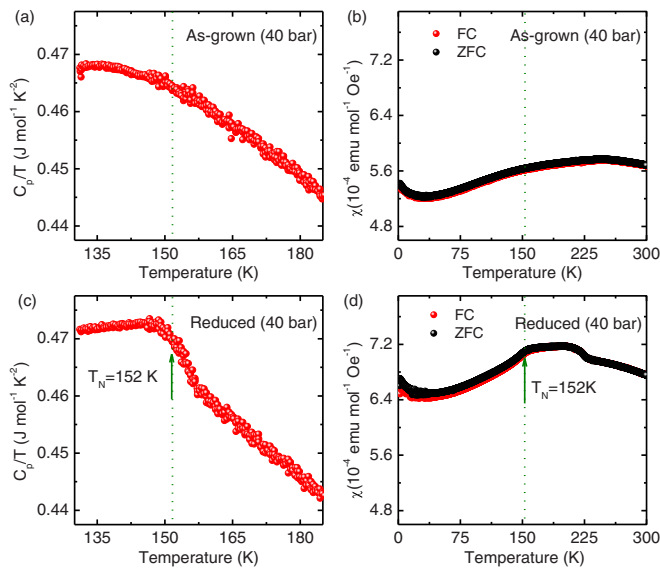
FIG. 2. Temperature dependence of the heat capacity and magnetic susceptibility of as-grown [(a) and (b)] ($\delta \sim 0.015$) and reduced [(c) and (d)] ($\delta \sim 0.076$) LaNiO$_{3-\delta}$ single crystal (pO$_2 = 40$ bar).

FIG. 3. Elastic neutron scattering intensity of the $(h,k,{}^{1}/_{4})$ scattering plane at 6 K for as-grown (a) ($\delta \sim 0.020$) and reduced (b) ($\delta \sim 0.079$) LaNiO$_{3-\delta}$ single crystal (pO$_2 = 130$ bar).

in Fig. 3 of the SM [40], where only superlattice reflections consistent with the presence of LaNiO$_{2.75}$ are visible. We therefore believe that the diffraction pattern from the area shown in Fig. 1(c) arises due to the presence of a mixture of both LaNiO$_{2.75}$ and LaNiO$_{2.5}$.

We now consider the magnetic susceptibility, χ, and heat capacity, C_p, of an as-grown $\sim$22.2 -mg crystal (grown under pO$_2 \sim 40$ bar), which are shown in Figs. 2(a) and 2(b). A broad maximum centered at $T \sim 200$ K, which is consistent with previous reports of as-grown crystals by Guo *et al.* [6] and Zhang *et al.* [28], was observed in χ. The origin of this broad feature is an open question, as is whether or not it is intrinsic to stoichiometric LaNiO$_3$. It is notable that earlier work on polycrystals evidenced a markedly different temperature dependence [5]. Heat capacity is featureless in the temperature range between 130 and 190 K. Thus neither C_p or χ indicate any evidence of structural or magnetic transitions for the as-grown crystal over this temperature range.

Figures 2(c) and 2(d) show identical measurements performed on the same 22.2-mg crystal specimen after reduction. It is immediately apparent that significant changes were induced by the reduction. In contrast to the as-grown crystal, χ rises below $T \sim 225$ K on cooling, reaches a plateau between 225 and 152 K, and then decreases below 152 K. Furthermore, a broad peak in C_p/T, which was not apparent in the as-grown crystal, is observed at $\sim$152 K. The increase in susceptibility below $T_C \sim 225$ K suggests a ferromagnetic ordering, while the decrease below $T_N \sim 152$ K implies AFM ordering. We note that the oxygen vacancy-ordered phase LaNiO$_{2.75}$ has been reported to be ferromagnetic with $T_C \sim$ 230 K [41], which implicates this impurity as the source of the ferromagnetic ordering observed in our LaNiO$_{3-\delta}$ specimen. Similarly, LaNiO$_{2.5}$ [35,36,39,42,44–50] has been reported to be AFM with $T_N \sim 140$ K [35]. The proximity of this reported T_N to that observed in our oxygen deficient crystal suggests that this impurity may be responsible for the apparent
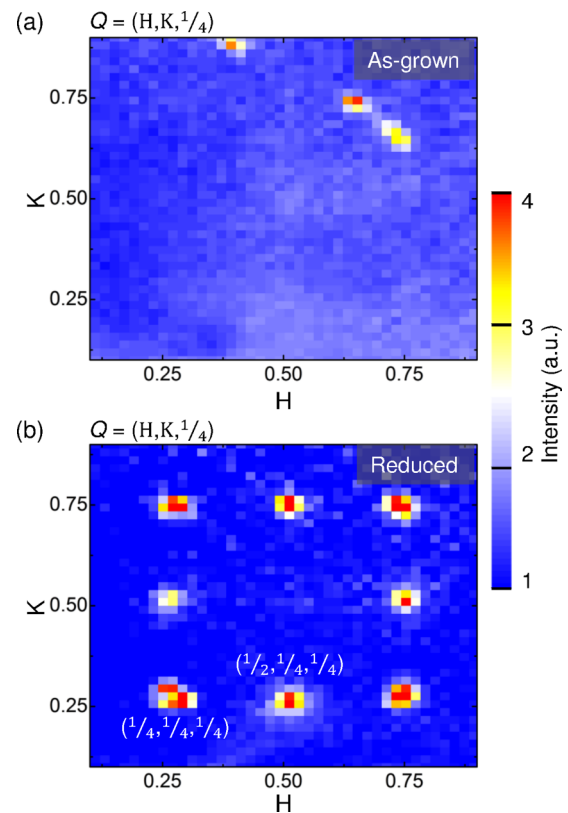
AFM transition. These bulk measurements therefore point to a scenario in which the reduction process increases the concentrations of regions of ordered oxygen vacancies possessing the LaNiO$_{2.5}$ and LaNiO$_{2.75}$ phases, which are present in dilute amounts in as-grown crystals. However, the nature of the reduction process likely leads to an inhomogeneous, core-shell-like structure in which the shell has a significantly higher oxygen vacancy concentration than the core. Although the line phases, LaNiO$_{2.5}$ and LaNiO$_{2.75}$, represent perfectly ordered lanthanum nickelate defect structures, there are certainly intermediate compositions that possess values of δ that are not precisely 0.5 and 0.25. As an example, Moriga *et al.* compared the magnetic properties of LaNiO$_{2.51}$ and LaNiO$_{2.54}$, and it appeared that the latter sample possessed a higher T_N [35]. It is logical to suspect that oxygen deficient regions with varying values of δ are present after reduction, and this likely leads to variance in T_N, which contributes to the broadness of the peak that we observed in C_p observed around 152 K after reduction.

Given the changes in magnetic behavior induced by reduction, we used single crystal neutron diffraction to further explore the magnetic ordering. Here, we focus on scattering from the single crystal grown under pO$_2$ of 130 bar (1.14 g); results from the single crystal grown under 40 bar are discussed further below. Figures 3(a) and 3(b) compare the pseudocubic $(h,k,{}^{1}/_{4})$ scattering plane of the 130 bar crystal before and after reduction. We note that the crystal was measured in the same sample environment for both measurements, and we have used
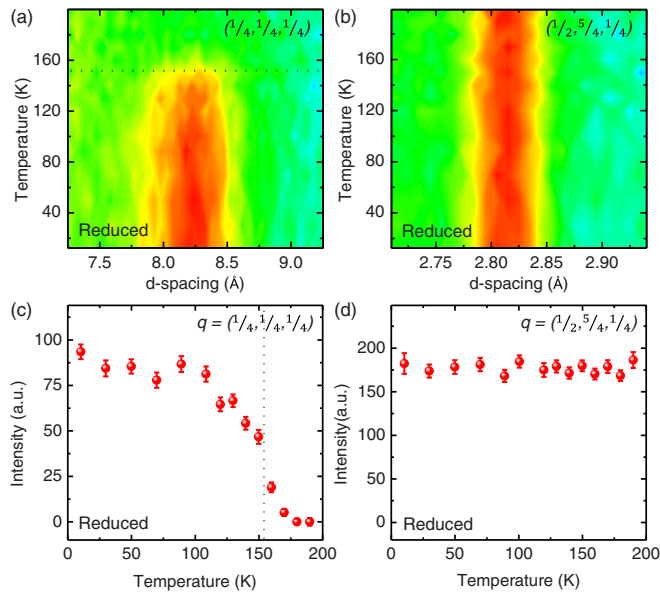
FIG. 4. Temperature dependence of the neutron intensity measured after reduction for [(a) and (c)] the $(^1/_4, ^1/_4, ^1/_4)$ peak and [(b) and (d)] the $(^1/_2, ^5/_4, ^1/_4)$ peak ($pO_2 = 130$ bar, $\delta \sim 0.079$).

nuclear Bragg reflections to normalize the intensities, allowing for direct comparison. Weak, temperature-dependent Bragg peaks indexed with a wave vector of $\boldsymbol{q}_m = (^1/_4, ^1/_4, ^1/_4)$ in pseudocubic notation are observed after reduction, but were not observable in the as-grown crystal. The temperature dependence of these peaks [Figs. 4(a) and 4(c)] evidences that they appear below approximately the same T_N observed in both χ and C_p, thereby confirming their AFM nature. The intensity of these peaks is enhanced by intentional reduction because the concentration of the oxygen vacancy-ordered regions is increased. That the density of the AFM defect structure regions increases after reduction in small pieces ($pO_2 = 40$ bar) as well as large ($pO_2 = 130$ bar) pieces implies a consistency in the transformation across processing conditions (regardless of size or initial growth pressure).

In addition to the temperature-dependent magnetic Bragg reflections discussed above, the reduction also induces structural modulations. From Figs. 3(a) and 3(b), it is apparent that peaks indexed with a wave vector of $\boldsymbol{q}_S = (^1/_2, ^1/_4, ^1/_4)$ are also present after reduction, but are below our detection limit in the measurement performed before reduction. These peaks are observed up to large values of $|\boldsymbol{Q}| = 10\,\text{Å}^{-1}$, suggesting that they are not of magnetic origin but rather arise from a structural modulation. Moreover, as shown in Figs. 4(b) and 4(d), these peaks are temperature-independent up to at least 200 K. Finally, we note that these peaks possess the same wave vector observed in the oxygen-vacancy ordered regions by TEM, which confirms that they are structural and arise due to oxygen vacancy ordering. The observed magnetic wave vector indicates that the magnetic unit cell is doubled along one pseudocubic axis with respect to this vacancy-ordered structure.

Other changes induced by reduction are observed at the pseudocubic Brillouin zone boundaries. Consider first the as-grown sample with a small concentration of defect regions. As shown in the intensity map of the $l = ^1/_2$ plane in Fig. 5(a),

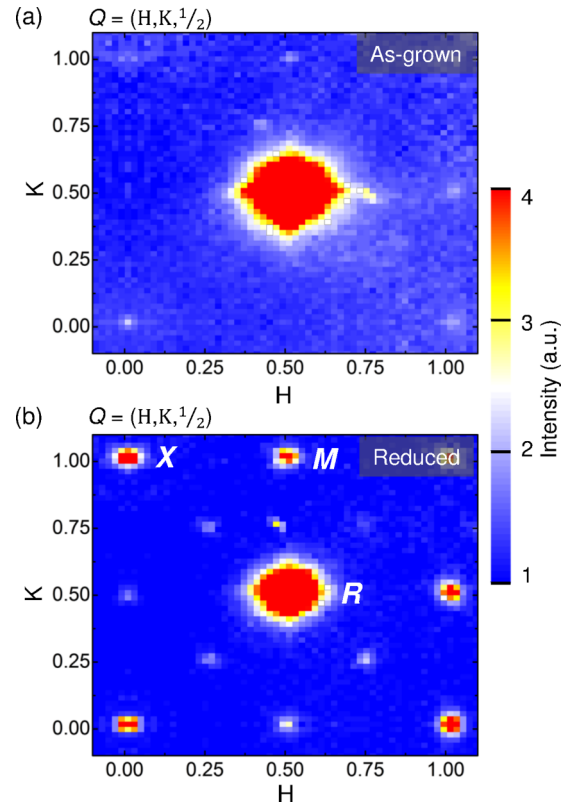FIG. 5. Elastic neutron scattering intensity of the $(h, k, ^1/_2)$ scattering plane at 6 K for as-grown (a) ($\delta \sim 0.020$) and reduced (b) ($\delta \sim 0.079$) LaNiO$_{3-\delta}$ single crystals ($pO_2 = 130$ bar).

we observed strong peaks at the R points and extremely weak peaks at X and M points. This evidences a dilute concentration of the oxygen-ordered phases which yield reflections at X and M in the as-grown sample, consistent with the TEM results described above. The reason that these are visible when the magnetic peaks are not is because their structure factors are intrinsically much larger than those of the magnetic peaks. Because of the dilute but finite concentration of ordered defect phases, it is impossible to use the observed scattering at the X and M points to support the claim that the rhombohedral (space group $R\bar{3}c$) symmetry is broken in stoichiometric LaNiO$_3$ [51]. Nevertheless, upon reduction, the scattering at the X and M points significantly increases, as shown in Fig. 5(b), consistent with an increasing phase fraction of the vacancy-ordered phases. Our neutron data provides no evidence of symmetry breaking of stoichiometric LaNiO$_3$, and given that the electron diffraction data in regions where ordered vacancies are not present [Fig. 1(b)] evidences only pseudocubic Brillouin zone boundary peaks at R and not X or M points, it is reasonable to conclude that the average structure of the ground state of stoichiometric LaNiO$_3$ is rhombohedral

IV. SUMMARY AND CONCLUSIONS

We summarize our findings as follows. The crystals that we have synthesized at pressures of 40 and 130 bar pO_2 tend to grow nearly stoichiometric, but there is a finite, nonzero concentration of oxygen vacancies ($\delta \sim 0.02$) present in spec-
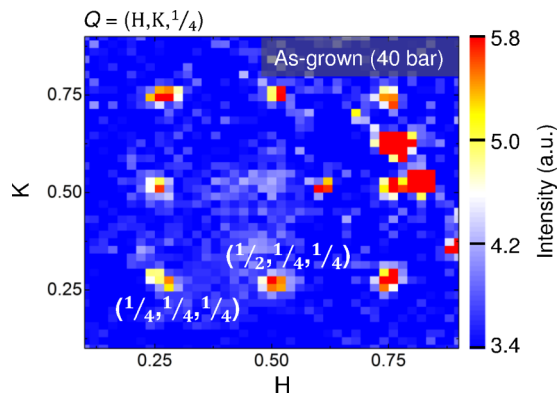
FIG. 6. Elastic neutron scattering intensity of $(h, k, 1/4)$ scattering plane at 6 K for an as-grown LaNiO$_{3-\delta}$ single crystal that had been grown under $pO_2 = 40$ bar ($\delta \sim 0.015$).

imens taken from as-grown boules in both cases. Microscopy clearly establishes that there is a tendency of these vacancies to form ordered defect regions, which appear to have LaNiO$_{2.5}$ and LaNiO$_{2.75}$ structures, and are AFM and ferromagnetic [35], respectively. Depending on their relative concentrations, these defect regions can easily lead to difficulties in interpreting the intrinsic properties of stoichiometric LaNiO$_3$ based on a single-crystal specimen. Because the concentrations may depend upon both the radial position (i.e., core or surface of the rod) as well as the position along the growth axis, it is important to realize that stoichiometry or lack of detectable impurities within a small piece removed from a rod may not reflect the overall composition of larger samples used for neutron scattering studies.

An example of the confusion in interpreting the results of a neutron scattering experiment is given in Fig. 6, which shows the neutron scattering pattern measured from another as-grown crystal (grown at pO_2 40 bar). In contrast to the measurements shown in Fig. 3(a), which had been performed on an as-grown crystal at pO_2 of 130 bar, we observed magnetic peaks at $\boldsymbol{q}_m = (1/4, 1/4, 1/4)$ from this particular crystal without reduction, even though TGA analysis performed on small pieces of boules grown under 130 bar and 40 bar yielded similar oxygen contents for as-grown crystals. Given that such peaks were only observed in the 130 bar crystal after intentional reduction, we conclude that the magnetic ordering wave vector was observable in the as-grown ($pO_2 = 40$ bar) crystal because this particular specimen has a larger concentration of the LaNiO$_{2.5}$ phase.

Concerning stoichiometric, bulk LaNiO$_3$, our measurements evidence nothing that contradicts the picture of a nonmagnetically ordered, metallic ground state. Nor do they confirm that the nonmagnetically ordered state is the ground-state because of the defects that are inherently present in our specimens. Instead, our results do confirm that AFM ordering is induced concomitant with ordered oxygen defect structures upon reduction of LaNiO$_{3-\delta}$ with hydrogen. There are two possibilities for reconciling the results of Guo *et al.* [6] with the present work. The first is that, as argued by Guo *et al.*, the AFM ground-state that they observed is an intrinsic property of LaNiO$_3$ that requires extremely pure samples that are stoichiometric (Guo *et al.* reported $\delta = 0.002$ as derived from the initial and final masses measured in TGA [6]). The

second is that the neutron-sized samples measured by Guo *et al.* may possess oxygen-ordered regions that were not observed in the TGA measurement which would have been performed on a much smaller specimen, in which case the antiferromagnetism would result from these regions. Ultimately, the present work cannot definitively distinguish between these two possibilities.

However, the present work does offer a mechanism by which these two possibilities could be resolved and by which future studies should be judged. We suggest that when future neutron scattering measurements are reported on single-crystal LaNiO$_3$, measurements over reciprocal space regions that contain M, X, and $(1/4, 1/4, 1/2)$ propagation vectors from the cubic Γ point should also be reported, since the present work shows that these are clearly nuclear peaks that are correlated with oxygen-deficient regions. If these points are absent in a sample that possesses an AFM Bragg peak, then we would argue that the antiferromagnetism is an intrinsic property of stoichiometric LaNiO$_3$; otherwise, the antiferromagnetism would originate from oxygen vacancy ordering.

Although we presently do not understand the broad maximum in the χ at 200 K, the decrease in χ upon cooling may perhaps be interpreted as evidence for fluctuating AFM correlations. If true, this behavior would represent a deviation from the conventional view of the system as being a Pauli paramagnet. However, as we asserted in Ref. [28], we cannot rule out the possibility that the small oxygen deficiency is behind this maximum, though measurements on polycrystals of LaNiO$_{2.5}$ and LaNiO$_{2.75}$ do not exhibit it [35,41]. Overall, our results highlight that stoichiometry should be carefully considered when interpreting the intrinsic physical properties of the rare-earth nickelates, particularly as new compositions continue to emerge with developing high-pressure floating-zone technology. The proposed bond disproportionation mechanism of the MIT in nickelates suggests that the transfer of charge between Ni cations and oxygen anions plays a pivotal role in the bulk electronic and magnetic properties of nickelates; as such, the presence of oxygen vacancies in nickelate samples is an important consideration. Finally, our results clearly demonstrate that topotactic reduction of perovskite nickelate single crystals is a viable means for investigating ordered oxygen vacancies and exploring the physics of these reduced phases.

[1] J. B. Torrance, P. Lacorre, A. I. Nazzal, E. J. Ansaldo, and C. Niedermayer, Phys. Rev. B **45**, 8209 (1992).

[2] J. L. García-Muñoz, J. Rodríguez-Carvajal, P. Lacorre, and J. B. Torrance, Phys. Rev. B **46**, 4414 (1992).

[3] J. A. Alonso, J. L. García-Muñoz, M. T. Fernández-Díaz, M. A. G. Aranda, M. J. Martínez-Lope, and M. T. Casais, Phys. Rev. Lett. **82**, 3871 (1999).

[4] I. I. Mazin, D. I. Khomskii, R. Lengsdorf, J. A. Alonso, W. G. Marshall, R. M. Ibberson, A. Podlesnyak, M. J. Martínez-Lope, and M. M. Abd-Elmeguid, Phys. Rev. Lett. **98**, 176406 (2007).

[5] J.-S. Zhou, L. G. Marshall, and J. B. Goodenough, Phys. Rev. B **89**, 245138 (2014).

[6] H. Guo, Z. W. Li, L. Zhao, Z. Hu, C. F. Chang, C.-Y. Kuo, W. Schmidt, A. Piovano, T. W. Pi, O. Sobolev, D. I. Khomskii, L. H. Tjeng, and A. C. Komarek, Nat. Commun. **9**, 43 (2018).

[7] A. S. Disa, F. J. Walker, S. Ismail-Beigi, and C. H. Ahn, APL Mater. **3**, 062303 (2015).

[8] M. Medarde, M. T. Fernández-Díaz, and P. Lacorre, Phys. Rev. B **78**, 212101 (2008).

[9] S. J. Allen, A. J. Hauser, E. Mikheev, J. Y. Zhang, N. E. Moreno, J. Son, D. G. Ouellette, J. Kally, A. Kozhanov, L. Balents, and S. Stemmer, APL Mater. **3**, 062503 (2015).

[10] S. Lee, R. Chen, and L. Balents, Phys. Rev. B **84**, 165119 (2011).

[11] R. J. Green, M. W. Haverkort, and G. A. Sawatzky, Phys. Rev. B **94**, 195127 (2016).

[12] H. Park, A. J. Millis, and C. A. Marianetti, Phys. Rev. Lett. **109**, 156402 (2012).

[13] S. Johnston, A. Mukherjee, I. Elfimov, M. Berciu, and G. A. Sawatzky, Phys. Rev. Lett. **112**, 106404 (2014).

[14] V. Bisogni, S. Catalano, R. J. Green, M. Gibert, R. Scherwitzl, Y. Huang, V. N. Strocov, P. Zubko, S. Balandeh, J. Triscone, G. Sawatzky, and T. Schmitt, Nat. Commun. **7**, 13017 (2016).

[15] T. Mizokawa, D. I. Khomskii, and G. A. Sawatzky, Phys. Rev. B **61**, 11263 (2000).

[16] J. Varignon, M. N. Grisolia, J. Íñiguez, A. Barthélémy, and M. Bibes, npj Quantum Mater. **2**, 21 (2017).

[17] A. Subedi, arXiv:1708.08899.

[18] J. Shamblin, M. Heres, H. Zhou, J. Sangoro, M. Lang, J. Neuefeind, J. A. Alonso, and S. Johnston, Nat. Commun. **9**, 86 (2018).

[19] B. Li, D. Louca, S. Yano, L. G. Marshall, J. Zhou, and J. B. Goodenough, Adv. Electron. Mater. **2**, 1500261 (2016).

[20] S. Lee, R. Chen, and L. Balents, Phys. Rev. Lett. **106**, 016405 (2011).

[21] L. Balents, Commentary in the Journal Club for Condensed Matter Physics (2017).

[22] J. B. Goodenough and P. M. Raccah, J. Appl. Phys. **36**, 1031 (1965).

[23] K. Sreedhar, J. M. Honig, M. Darwin, M. McElfresh, P. M. Shand, J. Xu, B. C. Crooker, and J. Spalek, Phys. Rev. B **46**, 6382 (1992).

[24] N. Y. Vasanthacharya, P. Ganguly, J. B. Goodenough, and C. N. R. Rao, J. Phys. C: Solid State Phys. **17**, 2745 (1984).

[25] W. C. C. Koehler and E. O. O. Wollan, J. Phys. Chem. Solids **2**, 100 (1957).

[26] J. A. Alonso, M. J. Martínez-Lope, M. T. Casais, J. L. García-Muñoz, and M. T. Fernandez-Diaz, Phys. Rev. B **61**, 1756 (2000).

[27] U. Staub, G. I. Meijer, F. Fauth, R. Allenspach, J. G. Bednorz, J. Karpinski, S. M. Kazakov, L. Paolasini, and F. d'Acapito, Phys. Rev. Lett. **88**, 126402 (2002).

[28] J. Zhang, H. Zheng, Y. Ren, and J. F. Mitchell, Cryst. Growth Des. **17**, 2730 (2017).

[29] Y. Kumar, A. P. Singh, S. K. Sharma, R. J. Choudhary, P. Thakur, M. Knobel, N. B. Brookes, and R. Kumar, Thin Solid Films **619**, 144 (2016).

[30] K. Tsubouchi, I. Ohkubo, H. Kumigashira, Y. Matsumoto, T. Ohnishi, M. Lippmaa, H. Koinuma, and M. Oshima, Appl. Phys. Lett. **92**, 262109 (2008).

[31] J. Son, J. M. Lebeau, S. J. Allen, and S. Stemmer, Appl. Phys. Lett. **97**, 202109 (2010).

[32] J. Son, P. Moetakef, J. M. Lebeau, D. Ouellette, L. Balents, S. J. Allen, and S. Stemmer, Appl. Phys. Lett. **96**, 062114 (2010).

[33] M. Gibert, M. Viret, A. Torres-Pardo, C. Piamonteze, P. Zubko, N. Jaouen, J. M. Tonnerre, A. Mougin, J. Fowlie, S. Catalano, A. Gloter, O. Stéphan, and J. M. Triscone, Nano Lett. **15**, 7355 (2015).

[34] M. Gibert, P. Zubko, R. Scherwitzl, J. Íñiguez, and J. M. Triscone, Nat. Mater. **11**, 195 (2012).

[35] T. Moriga, O. Usaka, T. Imamura, I. Nakabayashi, I. Matsubara, T. Kinouchi, S. Kikkawa, and F. Kanamaru, Bull. Chem. Soc. Jpn. **67**, 687 (1994).

[36] T. Moriga, O. Usaka, I. Nakabayashi, Y. Hirashima, T. Kohno, S. Kikkawa, and F. Kanamaru, Solid State Ionics **74**, 211 (1994).

[37] S. Rosenkranz and R. Osborn, Pramana - J. Phys. **71**, 705 (2008).

[38] F. Ye, Y. Liu, R. Whitfield, R. Osborn, and S. Rosenkranz, J. Appl. Crystallogr. **51**, 315 (2018).

[39] J. M. González-Calbet, M. J. Sayagués, and M. Vallet-Regi, Solid State Ionics **32–33**, 721 (1989).

[40] See Supplemental Material at http://link.aps.org/supplemental/10.1103/PhysRevMaterials.2.064404 to view the supplementary figures.

[41] T. Moriga, O. Usaka, I. Nakabayashi, T. Kinouchi, S. Kikkawa, and F. Kanamaru, Solid State Ionics **79**, 252 (1995).

[42] R. D. Sánchez, M. T. Causa, A. Caneiro, A. Butera, M. Vallet-Regí, M. J. Sayagués, J. González-Calbet, F. García-Sanz, and J. Rivas, Phys. Rev. B **54**, 16574 (1996).

[43] J. A. Alonso, M. J. Martínez-Lope, J. L. García-Muñoz, and M. T. Fernández, Physica B **234–236**, 18 (1997).

[44] K. Vidyasagar, A. Reller, J. Gopalakrishnan, and C. N. R. Rao, J. Chem. Soc., Chem. Commun. 7 (1985).

[45] J. A. Alonso, M. J. Martínez-Lope, J. L. García-Muñoz, and M. T. Fernández-Díaz, J. Phys.: Condens. Matter **9**, 6417 (1997).

[46] C. N. R. Rao, J. Gopalakrishnan, K. Vidyasagar, A. K. Ganguli, A. Ramanan, and L. Ganapathi, J. Mater. Res. **1**, 280 (1986).

[47] M. Abbate, G. Zampieri, F. Prado, A. Caneiro, J. M. Gonzalez-Calbet, and M. Vallet-Regi, Phys. Rev. B **65**, 155101 (2002).

[48] M. Crespin, P. Levitz, and L. Gatineau, J. Chem. Soc., Faraday Trans. 2 **79**, 1181 (1983).

[49] T. Moriga, S. Kikkawa, M. Takahashi, F. Kanamaru, and I. Nakabayashi, Jpn. J. Appl. Phys. **32-2**(Suppl.), 764 (1993).

[50] J. A. Alonso and M. J. Martínez-Lope, J. Chem. Soc., Dalton Trans. 2819 (1995).

[51] A. M. Glazer, Acta Cryst. B **28**, 3384 (1972).